Promotion of Perforation in a Radial Liquid Sheet by Impingement of a Hot/Cold Airflow

T. Wakimoto*, K. Nishida and K. Katoh
Department of Mechanical Engineering
Osaka City University
Osaka, 558-8585 Japan

Abstract

Promotion of perforations in a radial liquid sheet through hot/cold airflow is investigated. The radial liquid sheet was produced by release of a liquid film spreading on a disk into the air. In the radial liquid sheet, a turbulent transition occurs beyond the disk edge. The liquid sheet is perforated after the transition, and atomized by the perforations increasing with liquid sheet velocity. In this study, the promotion of the atomization by the hot/cold airflow was attempted. The hot/cold airflow impinged on the transition point at a velocity of 4-6m/s, and the perforation promoted by the hot/cold airflow was observed by photography. The difference $\Delta T=T_g-T_l$ between airflow temperature T_g and liquid sheet temperature T_l was controlled in the range from –20 to +135°C. Even the airflow with slight temperature difference ($\Delta T=\pm 15$°C) had potential of promoting the perforation, however, the airflow without temperature difference had no effect on the perforation. Critical conditions for the perforation promotion by the hot airflow are organized based on the observations of the liquid sheets under the various conditions of temperature difference and liquid sheet velocity. The photographs and organized critical conditions show that patchy thin liquid membranes, which are formed in places after the transition at high Reynolds numbers, is necessary for the perforation promotion. A mechanism was proposed for the perforation promotion by the hot/cold airflow based on a Marangoni stress affecting on the liquid membrane, which is heated/cooled easily because of its ultimate thinness. The beginning point of the perforation in the liquid membrane and the thickness of the liquid membrane are determined by CCD images of the liquid membrane. The difference in the beginning point of the perforation by airflow temperatures and measured thickness (about 5μm) of the liquid membrane support the validity of the proposed perforation mechanism.

1. Introduction

Several investigations have been conducted on the atomization characteristics of fuel injected in hot combustion chambers [1]-[4]. For example, Dombrowski and Foumeny[4] observed instability waves appearing on a liquid sheet injected from a fan spray nozzle to extremely hot combustion gas (=1000 °C), and revealed that a liquid sheet is perforated by high frequency waves, which develop instead of commonly observed Kelvin-Helmholtz waves[5]-[7] due to charged particles in the combustion gas. However, there is no experimental work that shows the influence of small temperature difference (about 20 °C) between liquid and gas on the behavior of a liquid sheet.

By contrast, we have investigated the turbulent transition of a radial liquid sheet, which is generated by releasing a liquid film on a disk into the air [8]-[10]. As the result, we have found that very thin liquid membrane forms in patches after the transition, and large number of perforations in the liquid membrane leads to liquid atomization. We have also found that the perforations are promoted by impingement of a hot airflow, which is 20 to 120 °C higher than liquid. In this study, we proposed a mechanism of the perforation, which is promoted by such small gas-liquid temperature difference, based on a Marangoni stress. We also proved the validity of the proposing mechanism from the measurements of the beginning point of the perforation and the thickness of the liquid membrane.

2. Experiment

The experimental setup used is illustrated in Fig. 1a. A radial liquid film was produced as water flowed radially outwards on a horizontal disk separated from the liquid delivery nozzle by a small gap. The diameter of the disk and the inner diameter of the nozzle were 60 and 25 mm, respectively. In the liquid film on the disk, a laminar velocity profile developed up to the liquid surface. The continued movement of the liquid film beyond the disk edge formed a radial liquid sheet. Upon ejection from the disk, the velocity profile in the radial liquid sheet varies from a laminar velocity profile to a velocity profile with an inflexion point due to the release of adhesion to the disk surface. This inflectional velocity profile leads to the turbulent transition.

*Corresponding author

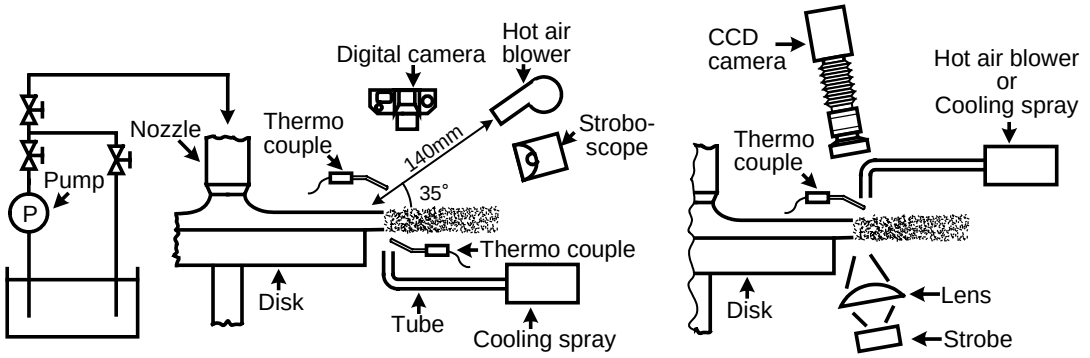

(a) Overview photography (b) Close-up photography

Figure 1. Experimental apparatus

The flow rate Q and the stagnation pressure P at the disk center were monitored during the experiment in order to estimate the liquid sheet thickness h_e and the surface velocity U_e at the disk edge. Additionally, the gap between the disk and nozzle was adjusted so that the liquid sheet thickness h_e maintained a constant value of 90 μm.

Flow conditions were specified by Reynolds number $Re=U_e h_e/\nu$ and Weber number $W_e=\rho h_e U_e^2/\sigma$, where ν, ρ and σ are kinematic viscosity, liquid density and surface tension, respectively. U_e and h_e were estimated on the assumption that the theoretical velocity profile proposed by Watson applied to the velocity profile of the liquid film on the disk [8]-[10]. During the experiments, U_e was controlled by the supply pressure of a pump, such that h_e=90 mm was maintained.

We used two types of camera configurations to take the overview photographs of the liquid sheet (Fig. 1a) and the close-up photographs of the very thin liquid membrane formed in the turbulent transition region (Fig. 1b). In the configuration for the overview photography, we located a digital camera and a strobe as shown in Fig. 1a. A hot air jet emerged from a hot air blower directed toward the disk edge, and impinged on the liquid sheet in the turbulent transition region. The diameter and velocity of the hot air jet was 35mm and 6m/s, respectively. A cold airflow was also generated with a cooling spray, which discharged a cold airflow at 0 °C using evaporation of a refrigerant (HFC-134a). The cold airflow was guided to the turbulent transition region through a pipe because the cold airflow ejected from the nozzle of the cooling spray easily diffused. The guide pipe was located beneath the liquid sheet not to hide the picture image of the liquid sheet. The velocity of the cold airflow at the pipe exit was 4m/s. We confirmed that the perforation promotion by the hot/cold airflow does not depend on the impingement direction of the airflow. When we made the cold airflow impinge on the upper surface of the liquid sheet, we were able to find no difference in the liquid sheet. The temperature of the hot/cold airflow was measured at 8mm downstream of the disk edge with two thermo couples mounted for two sides of the liquid sheet.

In the configuration for the close-up photography (Fig. 1b), we used a CCD camera with a high speed electronic shutter, which can take 2 sequential photo images (Hamamatsu photonics ICCD-7971, Exposure time:100ns, Frame interval time:10μs). In addition, a hot/cold airflow was guided to the upper side of the turbulent transition region through a pipe because the close-up photographic devices prevented hot/cold gas flow from outer side or downside. The velocity of the hot/cold airflow was 4m/s at pipe exit. The close-up photographs provided information about the beginning point and expansion speed of the perforation, which validated our proposing perforation mechanism.

3. Results and Discussion

3.1 Features of liquid sheet without airflow

Figures 2a to 2d show changes in features of the liquid sheet without an airflow by liquid surface velocity U_e. The temperatures of liquid and ambient air are same as 15°C. The scales over the figures indicate the distance x from the disk edge. At U_e=12 m/s (Fig. 2a), the liquid sheet is smooth and laminar. No characteristic feature such as perforations or turbulence is observed in Fig. 2a. At U_e=19 m/s, a turbulent transition occurs just beyond the disk edge (Fig. 2b). The liquid sheet surface whitens around the transition region since the liquid sheet is covered with fine granular waves. In addition, some perforations are observed downstream of the transition point. The perforations increase with increasing U_e (Fig. 2c). Large number of perforations leads to liquid atomization at quite large U_e (Fig. 2d).

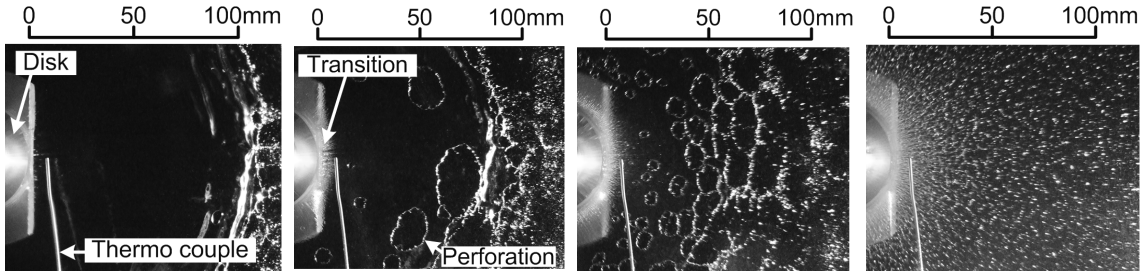

(a) U_e=12m/s, Re=950, We=180 (b) U_e =16m/s, Re=1240, We=310 (c) U_e =24m/s, Re=1890, We=700 (d) U_e =29m/s, Re=2270, We=1030

Figure 2. Overviews of liquid sheets without an airflow (T_l =15°C)

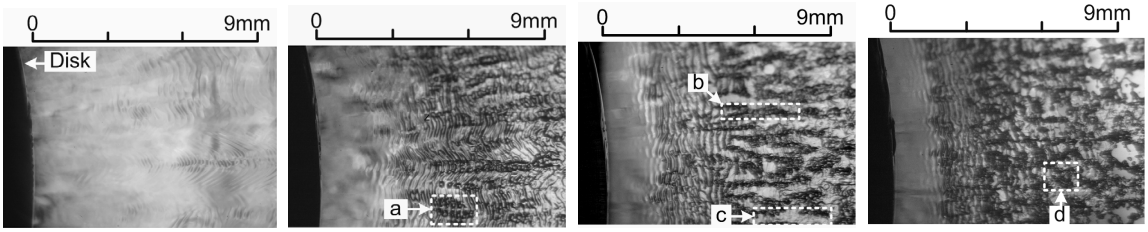

(a) U_e=12m/s, Re=950, We=180, Type A (b) U_e =16m/s, Re=1240, We=310, Type B (c) U_e =24m/s, Re=1890, We=700, Type C (d) U_e =29m/s, Re=2270, We=1030, Type D

Figure 3. Turbulent transition without an airflow (T_l =15°C)

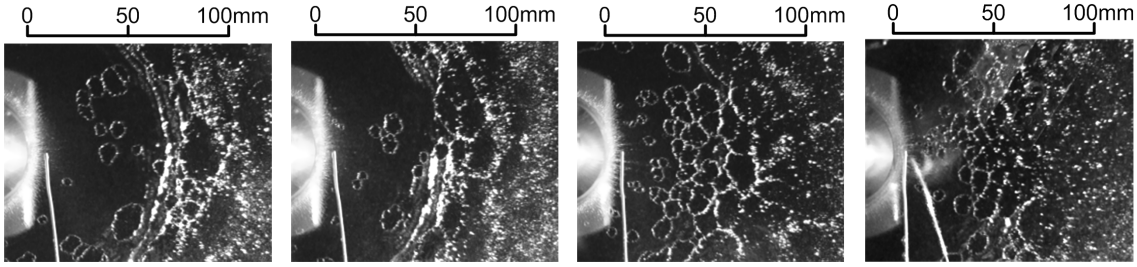

(a) Without air flow (b) ΔT =0°C (c) ΔT =15°C (d) ΔT =-15°C

Figure 4. Promotion of perforation by a hot/cold airflow (T_l =15°C, U_e=22m/s, Re=1750, We=600)

Detailed images in the transition regions corresponding to Figs. 2a to 2d are shown in Figs. 3a to 3d. Figures 3a to 3d were taken with the experimental apparatus in ref. [10]. The features of the transition regions were categorized into 4 types depending on U_e. Figure 3a shows a smooth surface as well as Fig. 2a (Type A). However, Fig. 3b shows concentric waves of about 0.3 mm wavelength in x=2-4 mm and spotted aggregations associated with the fine granular waves in x>4mm (a mark, Type B). In Fig. 3c, the aggregations become elongated like lines (b mark). In addition, strips of thin smooth liquid membrane are formed between the elongated aggregations (c mark, Type C). The perforation becomes remarkable in Fig. 2c because the rupture of the liquid membrane causes the perforation In Fig. 3d, the elongated aggregations become rather short and sigmoid (d mark, Type D). This complicated aggregation shape suggests that deformations such as bending or division occur in the elongated aggregations. Additionally, the deformation of the aggregation may induce frequent perforations in the thin liquid membrane present among the aggregations.

3.2 Promotion of perforation by hot/cold airflow

Figures 4a to 4d show the promotion of the perforation by a hot/cold airflow at liquid temperature T_l=15 °C, Re=1750 and We=600. Figure 4a represents a standard overview without an airflow. Figure 4b, 4c and 4d demonstrate overview images with air-liquid temperature difference ΔT=0, +15 and -15 °C, respectively, where ΔT is defined by subtraction of liquid temperature T_l from gas temperature T_g, that is $\Delta T = T_g - T_l$. Comparing Fig. 4b with Fig. 4a, the numbers of perforations in both figures are same. This indicates that the airflow without temperature differ-

ence has no effect on the perforation. In contrast, the number of perforations in Fig. 4c is larger than that in Fig. 4a. In Fig. 4d, the perforations are also promoted around the cooled point by a cold airflow. These figures indicate that perforation is promoted by the hot/cold airflow. Moreover, the promotion of perforation by a cold airflow implies that evaporation is not cause of the perforation promotion by a hot airflow.

We also observed the liquid sheet at T_l=35 °C, *Re*=2470 and *We*=500. Figures. 5a and 5b show the liquid sheets at ΔT =0 and 100 °C, respectively. We can find no difference between Fig. 5a and 5b regardless of much larger ΔT than that in Fig. 4. This means that perforation promotion by the hot airflow depends on flow condition. Hence, we determined the critical condition for the perforation promotion by observing the perforation at several T_g, T_l and U_e.

The comprehensive experimental result is shown in Fig. 6. A horizontal axis and vertical axis represent *Re* and *We*. The plots are the condition on which we observed. Thick solid lines in Fig. 6 represent critical flow conditions for the perforation promotion at ΔT =10, 30, 60 and 100 °C. The perforation is promoted by the hot airflow at higher Weber numbers than the solid lines. The solid lines shift to lower Weber number with increasing ΔT. This implies that a hot airflow with large temperature difference has strong promotion effect. In addition, the solid lines also shift to lower Weber number with decreasing liquid temperature. Therefore, the perforation is easily promoted by a hot airflow at low liquid temperature.

In the following sections, we consider the mechanism of the perforation promotion by a hot/cold airflow. As shown in Figs. 3c and 3d, very thin liquid membrane forms in the transition region. We reported that the perforation occurs in the liquid membrane under the condition of no airflow [10]. Hence, we consider the perforation of the liquid membrane by the hot/cold airflow as shown in Fig. 7. In the turbulent transition region, aggregations of the fine waves and strips of smooth liquid membrane are formed as shown in Fig. 7a (ref. Fig. 3c). When a hot airflow impinges on the liquid sheet, the temperature of the liquid membranes increases easily whereas the temperature of the aggregations still remains constant, because heat capacity of the liquid membranes is much smaller than that of the aggregations (Fig. 7b). The increase of the liquid membranes induces decrease of surface tension. As the result, surrounding aggregations pull the liquid membranes due to the difference of surface tension between the aggregations and liquid membranes. This Marangoni stress causes perforation in the center of the membranes. In contrast, when a cold airflow impinges on the liquid sheet, temperature decrease cause contraction of the liquid membrane (Fig. 7c). In this case, membrane is perforated at the edge of the membrane. Consequently, it is expected that the beginning point of the perforation in the liquid membrane is different de-

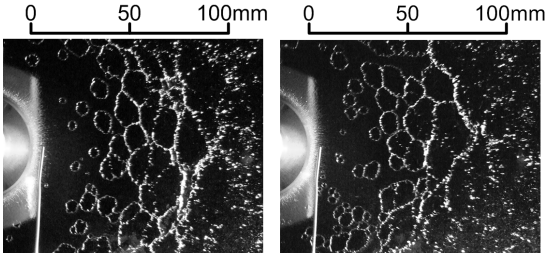

(a) ΔT =0°C (c) ΔT =100°C

Figure 5. Promotion of perforation by a hot/cold airflow (T_l =35°C, U_e=20m/s, *Re*=2470, *We*=500)

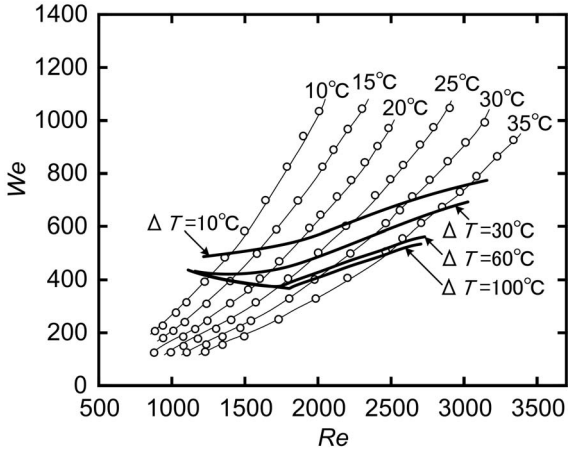

Figure 6. Critical flow conditions of promotion of perforation by a hot air flow

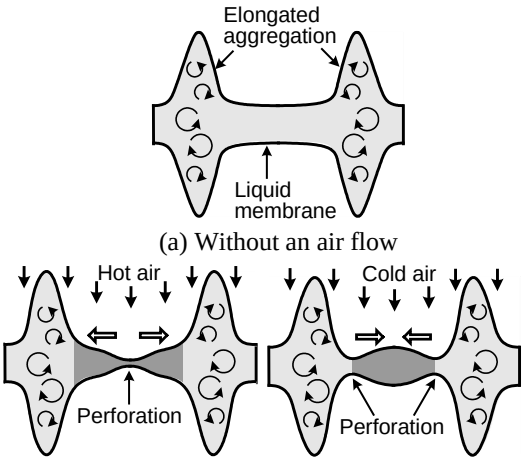

(a) Without an air flow

(b) With a hot air flow (c) With a cold air flow

Figure 7. Promotion of perforation by a hot/cold air flow

pending on the direction of temperature gradient.

To prove this assumption, we determined the beginning point of the perforation of the liquid membrane with close-up photographs. Figure 8a to 8c show the close-up photographs of the liquid membranes with no airflow, a hot airflow (ΔT=25°C) and a cold airflow (ΔT=-25°C), respectively. The schematics of the dotted line area in the close-up photographs are added on the right in Figs. 8a to 8c. Black, gray and white parts of the schematics illustrate the aggregations of the fine waves, liquid membranes and perforations, respectively.

In the case of no airflow, the liquid membrane is mainly perforated at the edge of the membrane as shown in Fig. 8a. In particular, perforations often observed near the micro projections extending from the aggregations to the liquid membranes. The movement of the micro projection probably induces the perforation because the deformation and bending of the micro projections are often observed. In the case of a hot airflow, the liquid membrane is not only perforated at the edge of the membrane, but also perforated in the center, as shown in Fig. 8b. On the contrary, the membrane is mainly perforated at the edge of the liquid membrane with a cold airflow regardless of the existence of the micro projections. This suggests that the perforation mechanism shown in Fig. 7 is valid.

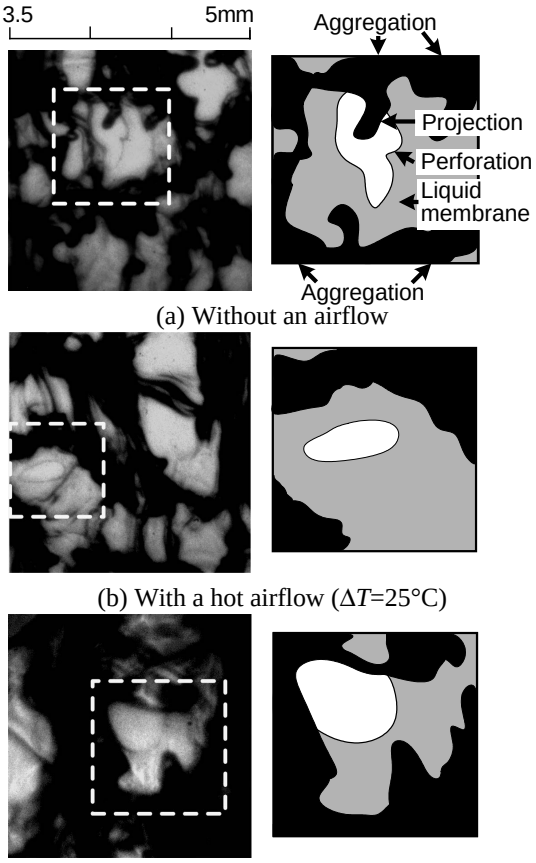

(a) Without an airflow

(b) With a hot airflow (ΔT=25°C)

(c) With a cold airflow (ΔT=-25°C)

Figure 8. Perforation in liquid membrane (T_l =25°C, *Re*=3190, *We*=1270)

3.3 Thickness of liquid membrane

In order to perforate according to the mechanism shown in Fig. 7, the temperature of the liquid membrane must be varied rapidly by heat transfer from a hot/cold airflow, hence, very small thickness of the liquid membrane is necessary for the perforation. Accordingly, we measured the thickness of the liquid membrane based on the expansion speed of the perforation in the following way.

Fraser proposed a theoretical expansion speed of a circular perforation expanding in an infinite liquid sheet with uniform thickness, considering the relationship between the surface tension affecting the edge of the perforation and the inertia force by excluded liquid mass [11]. The expansion speed dd_p/dt is expressed as following formula,

$$\frac{dd_p}{dt} = \sqrt{\frac{8\sigma}{h_m \rho}}, \qquad (1)$$

where h_m is the thickness of the liquid sheet. In this study, we estimated the thickness of the liquid membrane from the measured expansion speed of the perforation using formula (1). The expansion speed was measured with 2 sequential images taken at time interval Δt=10μs.

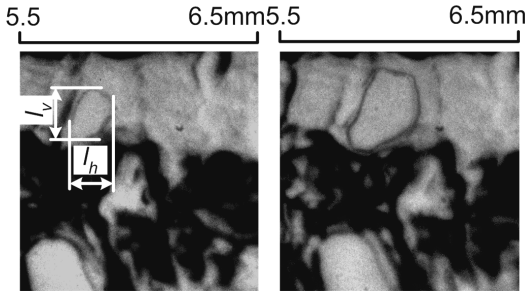

(a) First frame (b) Second frame (after 10 μs)

Figure 9. Expansion of a perforation (T_l =25°C, *Re*=3190, *We*=1270)

Figure 9a and 9b show the examples of the sequential images. We determined the perforation diameter d_p by averaging the vertical length l_v and horizontal length l_h of the perforation because the perforation is not always circular. The difference Δd_p between the diameters in the 2 images provides the expansion speed $\Delta d_p/\Delta t$. The estimated membrane thickness h_m at T_l =25°C is plotted against *Re* in Fig. 10. Each plot indicates the average of ten measured values, and error bars represent standard deviations.

Although measured values have large dispersion at especially low Reynolds numbers, ten times averaged value show the followings statistically. The liquid membrane thickness h_m at Re=1800, which nearly equals to the critical Reynolds number (=1700) for the creation of the liquid membrane (ref. Fig.4), is about 16μm. h_m decrease with increasing Re, and is reduced to about 5μm at Re=3120. This thickness comes to mere 5% of the liquid sheet thickness at the disk edge (h_e=90μm). The broken line in Fig. 10 indicate the critical Reynolds number for the promotion of the perforation by the hot airflow with ΔT=10°C (ref. Fig. 7); the perforation is promoted by the hot airflow over this critical Re. The liquid membrane thickness h_m at the critical Reynolds number is identical to about 7μm. The experimental results at different T_l also indicated that liquid membrane attenuated to be about 7μm at critical Reynolds number for ΔT=10°C. This means that slight temperature difference such as 10°C promotes the perforation when the liquid membrane thickness is quite small.

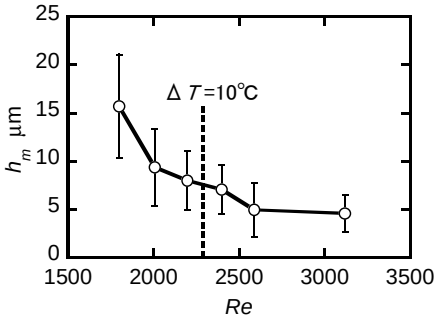

Figure 10. Thickness of liquid membrane (T_l=25℃)

4. Conclusions

We considered the perforation mechanism by a hot/cold airflow in the radial liquid sheet, which is formed by the release of a liquid film on a disk. The following conclusions were derived from the results and discussion.

1. The critical conditions of the liquid sheet and the airflow for the promotion by the hot airflow are revealed.
2. A cold airflow promotes the perforation as well as a hot airflow. This means that the perforation promotion by the hot airflow is not due to evaporation.
3. The hot airflow induces the perforation at the edge of the liquid membrane, which forms in the turbulent transition region of the liquid sheet. On the contrary, the cold airflow induces the perforation in the center of the liquid membrane.
4. The thickness of the liquid membrane decreases with increasing Re. When the liquid membrane thickness is reduced to about 7 μm, the liquid membrane is perforated by an airflow with slight temperature difference such as 10°C between air and liquid.
5. The perforation mechanism by the hot/cold airflow has been proposed based on a Marangoni stress. The validity of the proposed perforation mechanism has been proved by the measured thickness of the liquid membrane and the original perforation point depending on the direction of temperature gradient between an airflow and liquid.

References

1. Pal, S., et. al., *Atomization and Sprays*, 6 : 227-244 (1996).
2. Zhang, Y., et. al., *Atomization and Sprays*, 16 : 35-49 (2006).
3. Clark, C. J. and Dombrowski, N., *Journal of Fluid Mechanics*, 64 : 167-175 (1974).
4. Dombrowski, N. and Foumeny E. A., *Atomization and Sprays*, 8 : 235-240 (1998).
5. Hagerty, W. W. and Shea, J. F., *Journal of Applied. Mechanics*., 22 : 509-514 (1955).
6. Dombrowski, N. and Johns W. R., *Chemical Engineering Science*, 18 : 203-214 (1963).
7. Lienemann H., Shrimpton J. and Fernandes E., *Experimental in Fluids*, 42 : 241-258 (2007).
8. Wakimoto, T. and Azuma, T., *JSME International Journal, Series B*, 42-2 : 214-233 (1998).
9. Wakimoto, T. and Azuma, T., *5th International Conference on Multiphase Flow*, Yokohama, June 2004, No. 416 (CD-ROM).
10. Wakimoto, T. and Azuma, T., *Transactions of the Japan Society of Mechanical Engineers, Series B (in Japanese)*, 73-729 : 1205-1213 (2007).
11. Fraser, R. P., Eisenklam, P., Dombrowski, N. and Hasson D., *AIChE Journal* 8 : 672-680 (1962).